Journal of the Korean Association of Crystal Growth
Vol. 10, No. 2 (2000) 128-133

Two-dimensional continuum modelling of an inductively coupled plasma reactor

Dong Ho Kim, Won Young Chung* and Do Hyun Kim

Department of Chemical Engineering, KAIST, Taejon 305-701, Korea
**Semiconductor R&D Division, Samsung Electronics Co., LTD, Suwon 449-900, Korea*

(Received June 6, 1999)

Abstract Numerical analysis of the transport phenomena in an inductively coupled plasma reactor was conducted with the two-dimensional axisymmetric model including the electromagnetic field model, electron energy and species density models. The spatial distribution of the charged species in the bulk plasma and the ion flux to the wafer have been calculated to examine the influence of the process conditions including antenna and reactor geometry. The antenna radius had a significant influence on the plasma state and the axial ion flux distribution.

1. Introduction

A number of new plasma sources are being investigated and used in very-large-scale integrated circuits manufacturing. High plasma density ($>10^{11}\,cm^{-3}$) is required for high ion flux to surfaces, and hence high throughput in etching and film deposition processes [1]. Low neutral gas pressure (<10 mTorr) is necessary to ensure collisionless ion transport through sheaths for etching high aspect ratio features, such as trenches. Inductively coupled plasma (ICP) is one type of source that satisfies the above conditions, with the additional advantage of simplicity of design [2-4].

Modelling and numerical simulations of plasma processing can be useful in many ways. An improved understanding of a plasma processing system can be achieved by comparing predictions from numerical simulations with experimental observations. The optimization of existing processes or the development of new plasma processes that offer better processing results may follow such an understanding. Modelling and simulations based on reliable physical/chemical modelling of a plasma-processing system can significantly reduce the number of associated experiments. Additionally, such modelling and simulations can also be used in the computer-aided design (CAD) of new process systems and to optimize manufacturing processes within the framework of existing processing systems [5, 6]. Many ICP simulations reported so far have been based on the continuum or fluid approximation [3, 4, 7-9], which is also adopted in this study.

2. Modelling of ICP reactor

The model geometry of an ICP chamber chosen for numerical simulation is an axisymmetric cylindrical type reactor with planar coils. Several assumptions in the discharge model are employed to simplify the complex plasma system. Plasma state is assumed to be steady state and electrically neutral. Ambipolar diffusion is assumed so that the electron flux is equal to the ion flux. Energy change of neutral gas by viscous dissipation and compression is neglected. Our discharge model do not include the electrodynamics of plasma sheaths and the charged species motion in the sheaths, which must be resolved for complete understanding of etching or deposition processes on the substrates [10].

The computer simulation using the Galerkin finite element method begins with solving Maxwell's equations for electromagnetic field to determine the power deposition. This power deposition profile is used as input to the electron energy equation to determine the electron temperature. In turn these are used in the source term of species mass balance. These calculations are repeated until solutions are converged.

2.1. Electromagnetic model

The electromagnetic fields are obtained by solving Maxwell's equations in terms of the magnetic vector potential which has only the azimuthal component (A_θ) [11].

$$\nabla^2 A_\theta - \frac{1}{c^2}\frac{\partial^2 A_\theta}{\partial t^2} = -\mu_0 J, \qquad (1)$$

where c is the speed of light, J is the current density in the plasma and μ_0 is the permeability of the medium. The induced electric field in the plasma is given by

$$E_\theta = -\frac{\partial A_\theta}{\partial t}. \quad (2)$$

Replacing A_θ, J and E_θ by their phasor representations, ($A_\theta = \tilde{A}e^{jwt}$, $J = \tilde{J}e^{jwt}$ and $E_\theta = \tilde{E}e^{jwt}$) and recognizing that A_θ is only a function of (r, z) simplifies Eq. (1) to the partial differential equations in cylindrical coordinate. Boundary conditions are that $\tilde{A}_R$ and $\tilde{A}_I$ are zero along all the boundaries except at the top of the chamber where $\tilde{A}_R$ is nonzero. The variation of $\tilde{A}_R$ at the top of the chamber is obtained by applying the Biot-Savart law to each loop of the antenna [11-12]. The vector potential due to each turn of the antenna is given by

$$\tilde{A}_{R,j} = \frac{\mu_0 I a}{4\pi}\int_0^{2\pi}\frac{\cos\phi d\phi}{R}, \quad (3)$$

where I is the amplitude of the RF (Radio Frequency) current through each turn of the antenna and is the radius of the loop. R is the distance between the antenna of the loop and the boundary position and varies with ϕ:

$$R^2 = r^2 + d^2 + a^2 - 2ra\cos\phi, \quad (4)$$

where d is the distance between an antenna and the discharge/quartz window interface, that is, the thickness of the dielectric cap.

The power deposited from antennas is given by

$$P_{ext} = \frac{1}{2}\mathrm{Re}(\sigma_P|\tilde{E}|^2). \quad (5)$$

Electrons are heated by this inductive coupling by currents that are induced inside the plasma by time varying currents in the RF coils. In addition, there may be capacitive coupling in which plasma electrons respond to RF voltages on the inductive coil and chuck [13]. Capacitive coupling is not considered in the present model because that is usually a secondary heating process in ICP processes.

2.2. *Electron energy model*

The electron energy balance is

$$\nabla\cdot q_e + e J_e \cdot E - P_{ext} + P_{coll} = 0, \quad (6)$$

Table 1
Reaction set of Ar discharge

Reaction	H_j (eV)	Rate coefficient (cm^3/s)
$Ar + e \rightarrow Ar^+ + 2e$	17.7	$1.0\times10^{-7}\exp(-17.7/T_e)$
$Ar + e \rightarrow Ar^* + e$	11.6	$5.0\times10^{-9}\exp(-11.6/T_e)$
$Ar^* + e \rightarrow Ar^+ + 2e$	4.14	$2.05\times10^{-7}\exp(-4.95/T_e)$
$Ar^* + e \rightarrow Ar + e$	-11.56	2.0×10^{-7}
$Ar^* + Ar^* \rightarrow Ar^+ + Ar + e$	-	6.2×10^{-10}

with the electron energy flux given by

$$q_e = -K_e\nabla T_e + \frac{5}{2}kT_eJ_e, \quad (7)$$

where the thermal conductivity of electron is $K_e = 3/2\ kT_eD_en_e$. P_{coll} accounts for energy loss due to all electron collisions:

$$P_{coll} = 3\frac{m_e}{m_n}n_e v(kT_e - kT) + \sum_j H_jR_j. \quad (8)$$

Here, R_j denotes the j-th reaction rate and H_j is the energy loss due to j-th reaction, which are given in Table 1. Boundary conditions are that the electron energy flux on the walls is zero because we assume that the secondary electron flux is zero.

2.3. *Species density model*

The ambipolar diffusion-reaction model is used for obtaining the electron density distribution. The mass balance of electron at steady state is

$$\nabla\cdot J_e - \sum_j R_j = 0 \quad (9)$$

The electron flux is the superposition of the diffusion due to concentration gradient and the drift due to the electric field. J_e is given the by

$$J_e = -D_a\nabla n_e, \quad (10)$$

where D_a is the ambipolar diffusion coefficient given by

$$D_a = \frac{\mu_i D_e + \mu_e D_i}{\mu_i + \mu_e}. \quad (11)$$

Then, the electrostatic plasma field, E_s, is expressed by

$$E_s = -\nabla V_s = \frac{D_i - D_e}{\mu_i + \mu_e}\frac{\nabla n}{n}, \tag{12}$$

where V_s is the electrostatic plasma potential.

The electron flux on the walls is equal to the thermal flux perpendicular to the walls. Since the thermal speed is very high, the electron density on the walls is nearly zero. The continuity equation of meta-stable atom is expressed similar to that of the electron.

3. Result and discussion

Numerical simulations have been conducted to examine the influence of the process conditions and antenna geometry on the plasma state and ion flux distribution to the wafer with argon gas. The simulations were performed based on the reactor geometry described in Fig. 1, where chuck radius (R1), chamber radius (R2), chuck height (H2) and distance between inlet and chuck (H1) were set at 11.9 cm, 14 cm, 3.5 cm, and 7 cm, respectively. Solutions of the governing equations were obtained for the standard case of which conditions are listed in Table 2.

The contours of the azimuthal electric field for the standard case are presented in Fig. 2 (a). Because the electric field is induced by the time-varying magnetic field around the antenna coil, its distribution is very non-uniform and it has a peak at the antenna location. The maximum electric field is 1.851 V/cm at the top of the chamber in the same radial position with the radius of antenna and decays rapidly away from the antenna. With the induced electric field the power deposition profile can be determined, as shown in Fig. 2 (b). The power deposition is concentrated around coil and the total power absorbed in the plasma is about 200 W.

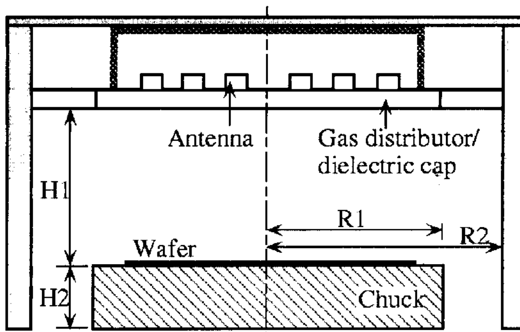

Fig. 1. ICP reactor with planar coils.

Table 2
Standard process condition

Descriptions	Values
Chamber pressure	10 mTorr
Number of antenna	1
Antenna radius	7 cm
Thickness of dielectric cap	1 cm
Antenna current	33.475 A
Frequency	13.56 MHz

In ICP reactor electrons are heated by the induced electric field and absorb power from the antenna coil, so that the non-uniform electric field distribution results in non-uniform electron temperature distribution and plasma generation. Electron temperature and plasma density distributions are shown in Fig. 2 (c) and (d). The maximum electron temperature is 3.185 eV at the peak of the electric field. In spite of power deposition being limited to the region directly below the coil, the long mean free path for electron transport produce fairly warm electrons. The electron density has the maximum value of $3.78\times10^{11}/cm^3$ that appears at 3.5 cm below the quartz plate on the axis of the chamber. For this relatively large chamber aspect ratio the plasma density peaks at the center of the discharge, since electron and ion transport are dominated by the large radial ambipolar diffusion gradients. In the other ext- reme, where the transport is dominated by the large axial ambipolar diffusion gradients, the plasma density peaks off-axis. Thus, there is an optimal chamber aspect ratio with which the ion flux distribution to the wafer is the most uniform. Electron density decays toward the walls. However, in contrast to the low-plasma-density capacitively coupled reactors, the electron density is quite high even very near the wall [8].

Ion flux to the wafer calculated from the obtained solutions for the standard case is in the range of 6~16 mA/cm^2. This distribution shows good uniformity in the central region up to the radius of 5 cm but the ion flux decreases with the radius. Near the wafer edge, the ion flux is about 43 % of the flux at the center.

Antenna coil placement, above all other design variables, directly affects the plasma state. Power deposition occurs dominantly in the proximity of the coil, and the distribution of electron source reaction rate can be controlled by changing the coil placement. To demonstrate the effect of coil placement on the plasma state, the numerical simulations were performed for

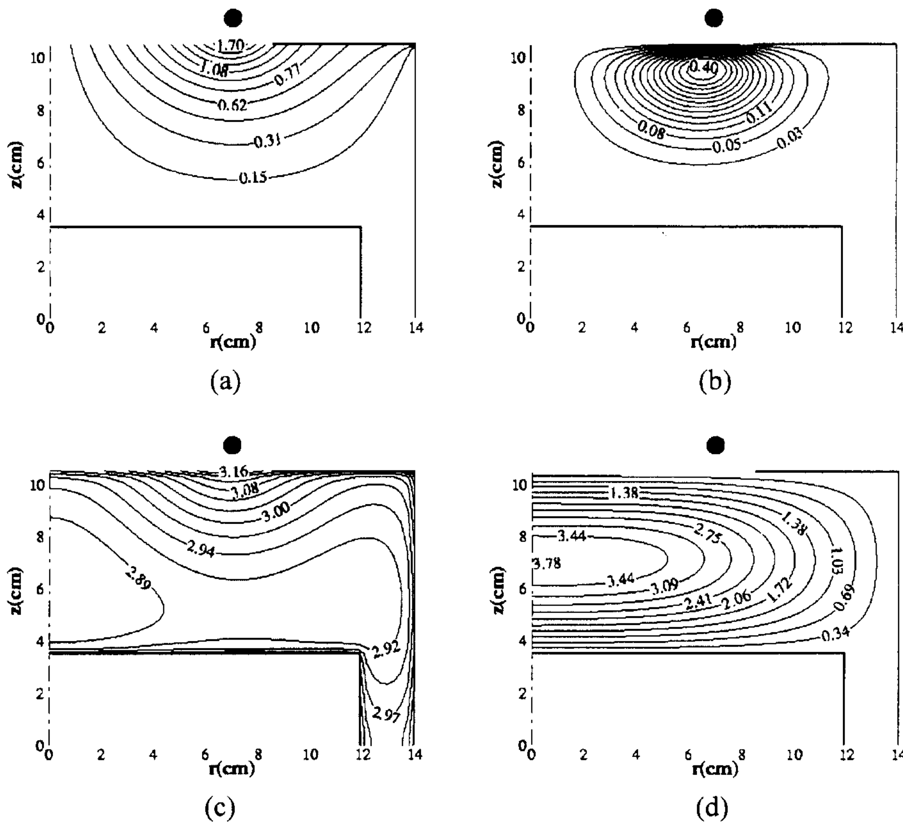

Fig. 2. Solutions of model equations for the standard case. (a) Induced azimuthal electric field distribution (V/cm), (b) power deposition (W/cm^3), (c) electron temperature distribution (eV), and (d) electron density ($\times 10^{11}$/cm^3).

various antenna radius. As the radius of the coil increases, the reaction rate of the electron generation increases and the peak point of these values migrates from the center region toward the reactor wall.

Decreasing the thickness of dielectric cap improves the coupling of plasma with the antenna, but it may increase the undesirable capacitive coupling between the antenna and the plasma.

The electron temperature is proportional to the absorbed power and the peak density is shown to

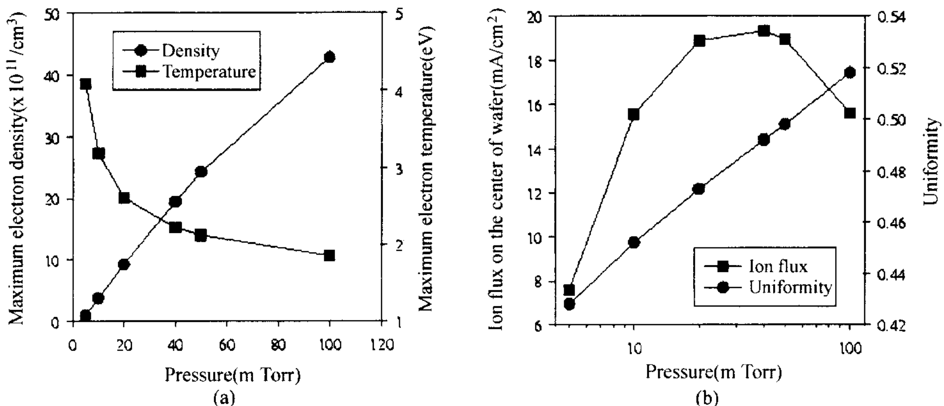

Fig. 3. Effect of operating pressure on (a) the maximum electron density and temperature and (b) the axial ion flux to the center of wafer and the uniformity of the ion flux.

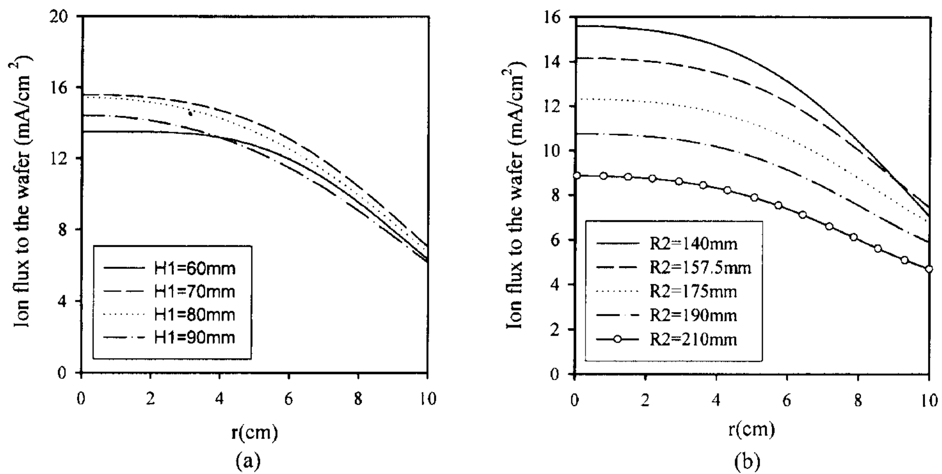

Fig. 4. Effect of reactor dimensions on the ion flux distribution (a) chamber height and (b) chamber radius.

increase linearly with the power deposition. Thus, the axial ion flux increases linearly with power deposition in the same way.

The reactor pressure is an important factor in the operating condition because the pressure affects the reaction rate, its uniformity and the properties of the thin film in the deposition and etching processes. In order to investigate the effect of operating pressure on the ion flux and its distribution, simulations are performed for pressure in the range from 5 to 100 mTorr. Peak electron density and temperature for various pressures are shown in Fig. 3 (a). The electron density increases linearly with the operating pressure, but the electron temperature decreases due to the increased energy loss by the collision with the neutral gas. Figure 3(b) shows the axial ion flux at the center of wafer as a function of the operating pressure and the uniformity which is defined as the ratio of the axial ion flux at the edge of the wafer to that at the center.

The ion flux uniformity increases a little with the pressure due to the migration of the peak point of the electron density toward the chamber wall but the ion flux has the maximum value with increasing pressure. Although the high pressure can improve uniformity, it is not desirable because the ion transport through sheaths becomes more collisional and the neutral gas temperature increases as the pressure increases (maximum gas temperature = 251°C at P = 50 mTorr). Therefore, there is an optimal operating pressure depending on process restrictions.

The reactor dimensions such as the chamber size and the aspect ratio have important effects on the plasma state and the ion flux uniformity to the substrate. The numerical simulations were carried out with changing the chamber height and radius. The simulation results for the ion flux to the wafer are presented in Fig. 4. The chamber height was found to have little influence on the ion flux under the standard conditions because with larger chamber height the more ions may be generated and transferred to the wafer but this increase is compensated with the diffusional losses on the chamber wall surface. But the radius of chamber was found to have more significant effects on the amount of ion flux and its uniformity. As the chamber diameter increased, the amount of ion flux to the wafer was decreased due to the radial diffusion and its uniformity slightly improved. Although the optimum size and aspect ratio of chamber could be determined with these calculations, that is strongly dependent of the type and placement of antennas.

4. Conclusions

Plasma model including the electomagnetic field, electron energy and density field equations based on the fluid approximation was built for the computer simulation of an inductively coupled plasma process.

The plasma state in the discharge and ion flux to the wafer were strongly dependent on the location of antenna coil. Power deposition was limited to the region directly below the coil, where electron temperature has its maximum of 3.185 eV. The electron density peaks at the center of the discharge and has the maximum value of $3.78 \times 10^{11}/cm^3$. The electron den-

sity increases linearly with the operating pressure but the electron temperature decreases. The reactor dimensions also affect the plasma state and the radius of chamber has significant effects on the amount of ion flux and its uniformity.

The results suggest that our fluid models can become useful tools for determining the optimum operation conditions and coil configuration.

References

[1] M.A. Lieberman and A.J. Lichtenberg, Principles of Plasma Discharges and Materials Processing, (John Wiley & Sons, Inc., New York, 1994) p. 19.
[2] J.C. Forster and J.H. Keller, High Density Plasma Sources, O. A. Popov, (Noyes Publication, New Jersey, 1995) p. 76.
[3] R.A. Stewart, P. Vitello and D.B. Graves, J. Vac. Sci. Technol. B 12 (1994) 478.
[4] R.A. Stewart, P. Vitello, D.B. Graves, E.F. Jaeger and L.A. Berry, Plasma Sources Sci. Technol. 4 (1995) 36.
[5] S. Hamaguchi, IBM J. Res. Develop. 43 (1999) 199.
[6] M.J. Kushner, Solid State Technology, June (1996) 135.
[7] D.P. Lymberopoulos and D.J. Economou, J. Appl. Phys. 73 (1993) 3668.
[8] D.P. Lymberopoulos and D.J. Economou, IEEE Trans. Plasma Sci. 23 (1995) 573.
[9] R.S. Wise, D.P. Lymberopoulos and D.J. Economou, App. Phys. Lett. 68 (1996) 2499.
[10] P.A. Miller and M.E. Riley, J. Appl. Phys. 82 (1997) 3689.
[11] A.P. Paranjpe, J. Vac. Sci. Technol A 12 (1994) 1221.
[12] F. Dai and C.H. Wu, IEEE Trans. Plasma Sci. 23 (1995) 65.
[13] E.F. Jaeger, L.A. Berry, J.S. Tolliver and D.B. Batchelor, Phys. Plasmas 2 (1995) 2597.